Coupled Electromagnetic-Thermal-Fluidic Analysis of Permanent Magnet Synchronous Machines with a Modified Model

Gaojia Zhu, Xiaoming Liu, Longnv Li, Hai Chen, and Jianguo Zhu, *Senior Member, IEEE*

***Abstract*—The researches on the heat generation and dissipation of the permanent magnet synchronous machines (PMSMs) are integrated problems involving multidisciplinary studies of electromagnetism, thermomechanics, and computational fluid dynamics. The governing equations of the multi-physical problems are coupled and hard to be solved and illustrated. The high accuracy mathematical model in the algebraically integral conservative forms of the coupled fields is established and computed in this paper. And the equation coupling with the fluid flow and the temperature variation is modified to improve the positive definiteness and the symmetry of the global stiffness matrix. The computational burden is thus reduced by the model modification. A 20kW 4500rpm permanent magnet synchronous machine (PMSM) is taken as the prototype, and the calculation results are validated by experimental ones.**

***Index Terms*—Cell method (CM), model modification, multi-physics coupled problems, permanent magnet synchronous machine (PMSM).**

I. Introduction

PERMANENT magnet synchronous machines (PMSMs) manifest superior advantages of high efficiency, high torque density and fast dynamics, and thus been widely applied to modern civil and industrial equipment. Since the PMSMs are mostly supplied from pulse-width modulation (PWM) controlled inverters [1], there exists large amounts of time harmonics inside the motor components which will generate eddy-current and hysteresis losses. Once overloaded, the elevated temperature rises introduced by the losses may cause accelerated aging of the winding insulation [2], diminish the magnetic properties of the PMs [3], and limit the torque output.

In order to maintain the temperature rise and maximize the output power, it is necessary to accurately predict the temperature distribution of the motor in the design process. The thermal analyses of the PMSMs evolved from the lumped parameter thermal networks (LPTNs) [4] to the field analysis methods [5]. Nowadays, the precise calculations of the multi-physical problems coupling electromagnetic-thermal-fluidic fields are gaining more and more research attentions since the electromagnetic losses are the main parts of the heat sources and the heat dissipation capacity is directly affected by the fluid flow distribution.

The cell method (CM) proposed by Enzo Tonti [6] is the computational method based on the previous works of the direct algebraic formulations of physical laws [7]. In CM based analyses, the computing regions are tessellated into dualized space-time structures forming the cell-complexes [8]. Compared with other methods, the CM demonstrates the conservation equations on the dual cell-complexes through the replacement of physical relations with the dimensional and dual relations of the cells. And the formulas declaring physical laws are translated into the conversions of global variables defined on nodes, edges, faces, and volumes.

In this paper, the algebraic-formed governing equations of the multi-physics problems is illustrated. The 2-D transient electromagnetic field is weakly coupled to the 3-D steady-state temperature field, while the thermal-fluidic problem is solved as a directly coupled system. The mathematical model representing the relations between the heat transferred by convection and the flow distribution is modified to improve the definiteness and the symmetry of the global stiffness matrix by the introduction of a first order error. And the calculation results are validated by experiments.

II. Multi-physics Models

In the CM based problems, the common dual forms are demonstrated as shown Fig. 1. And in Fig. 2, P_o and P_h are the points of the primal space corresponded to the volumes and $\tilde{V}_h$ of the dual one. Similarly, the primal lines L, faces S, and volumes V are related to the dual $\tilde{S}$, $\tilde{L}$, and $\tilde{P}$, respectively [8]-[9]. The transformation of the physical quantities in the same set of grids is named as the topological transformation while mathematically exhibited as the topological matrix $\boldsymbol{G}$, $\boldsymbol{C}$, and $\boldsymbol{D}$ in primal grids and $\tilde{\boldsymbol{G}}$, $\tilde{\boldsymbol{C}}$, and $\tilde{\boldsymbol{D}}$ in dual grids. Due to the duality, the topological matrices should obey the correlation equations [10]

$$\tilde{\boldsymbol{D}} = -\boldsymbol{G}^{\mathrm{T}} \tag{1}$$

$$\tilde{\boldsymbol{C}} = \boldsymbol{C}^{\mathrm{T}} \tag{2}$$

Manuscript was submitted for review on 29, April, 2018.

This work was supported in part by the National Natural Science Foundation of China under Grant 51337001 and 51777136.

G. J. Zhu, X. M. Liu, L. N. Li, and H. Chen are with the Key Laboratory of Advanced Electrical Engineering and Energy Technology, Tianjin Polytechnic University, Tianjin, 300387 China (e-mail: zhugaojia@tjpu.edu.cn).

J. G. Zhu is with the School of Electrical and Information Engineering, The University of Sydney, Sydney, Australia(e-mail: jianguo.zhu@sydney.edu.au).

Digital Object Identifier 10.30941/CESTEMS.2019.00027

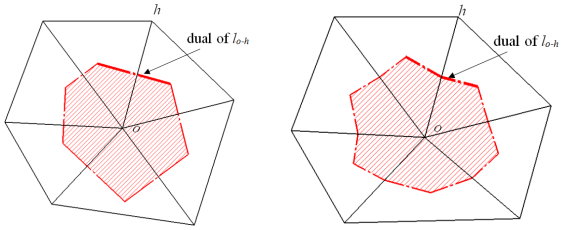

(a) circumcenter dual (b) barycentric dual

Fig. 1. Dual forms.

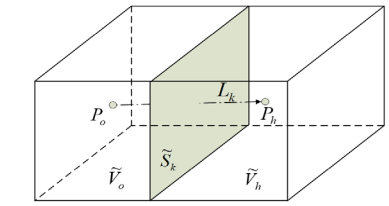

(a) dual relations of space

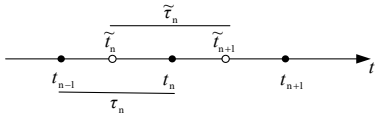

(b) dual relations of time

Fig. 2. Dual relations.

$$\tilde{\boldsymbol{G}} = \boldsymbol{D}^{\mathrm{T}} \tag{3}$$

Where $\boldsymbol{G}$, $\boldsymbol{C}$, $\boldsymbol{D}$ records the point-line, line-face, face-volume characters of the primal grids, and $\tilde{\boldsymbol{G}}$, $\tilde{\boldsymbol{C}}$, $\tilde{\boldsymbol{D}}$ of the dual ones. Moreover, the transformation between quantities defined on different sets of grids is named as the constitutive transformation which could mathematically expressed as the constitutive matrix $\boldsymbol{M}$ [11]-[12].

A. 2-D Electromagnetic Model

While dealing with the numerical problems, the CM based variables could be defined on points, lines, faces, and volumes, and thus enhancing the flexibility for the variables of multiple fields could be set on different dimensions of the cell-complexes. Since the working frequencies of most electromagnetic devices are well below 10^{10}HZ, the governing equations of quasi-stable electromagnetism are well developed with the neglect of the displacement currents as [13-14]

$$\begin{cases} \boldsymbol{C}^{\mathrm{T}}\boldsymbol{M}_{\mu}\boldsymbol{C}\boldsymbol{a} + j\omega\boldsymbol{M}_{\sigma}\boldsymbol{a} + \boldsymbol{M}_{\sigma}\boldsymbol{G}\boldsymbol{\chi} = \boldsymbol{M}_{S}\boldsymbol{J}_{s} \\ j\omega\boldsymbol{G}^{\mathrm{T}}\boldsymbol{M}_{\sigma}\boldsymbol{a} + \boldsymbol{G}^{\mathrm{T}}\boldsymbol{M}_{\mu}\boldsymbol{G}\boldsymbol{\chi} = 0 \end{cases} \tag{4}$$

where $\boldsymbol{a}$ is the line integral for magnetic vector potential, $\boldsymbol{J}_s$ the source current density, χ the electric scalar potential defined on points. For 2-D electromagnetic cases, χ satisfy the Laplace's equation and can be eliminated from the expression of the eddy currents, the transient governing equation is simplified as

$$\boldsymbol{K}_e\boldsymbol{a}(t_i) = \left[\boldsymbol{C}^{\mathrm{T}}\boldsymbol{M}_{\mu}\boldsymbol{C} + \frac{\boldsymbol{M}_{\sigma}}{\Delta t}\right]\boldsymbol{a}(t_i) = \boldsymbol{M}_{S}\boldsymbol{J}_{s}(t_i) + \boldsymbol{M}_{\sigma}\frac{\boldsymbol{a}(t_{i-1})}{\Delta t} \tag{5}$$

Where, i and i-1 are the serial numbers of time, Δt is the time step. The global stiffness matrix $\boldsymbol{K}_e$ is positive defined and symmetric.

B. 3-D Thermal Model

Through the transformation of the temperature defined on the primal points to the heat generated set in the dual volumes, the mathematical model of the CM based thermal problems can be formulated as [15]

$$\boldsymbol{K}_t\boldsymbol{T} = \boldsymbol{G}^{\mathrm{T}}\boldsymbol{M}_{\lambda}\boldsymbol{G}\boldsymbol{T} = \boldsymbol{q} \tag{6}$$

where $\boldsymbol{T}$ stands for the discrete vector of temperature, $\boldsymbol{M}_{\lambda}$ the constitutive matrix connecting primal lines and dual faces containing the information of grid dimensions and thermal conductivity coefficients, and $\boldsymbol{q}$ the heat vector. For the bearing regions of the machine, the elements of $\boldsymbol{q}_f$ are the frictional losses as

$$\boldsymbol{q}_f(m) = \frac{k_f V(m) g_r d_{sh} n}{\sum V(m)} \tag{7}$$

where k_f is the constant, $V(m)$ the volume of the grid m, g_r the quality of the rotor, d_{sh} the shaft diameter, n the rotate speed. The I^2R losses including the copper loss and the eddy-current loss can be expressed as

$$\boldsymbol{q}_R = \boldsymbol{M}_R\left[J^2\right] = \boldsymbol{M}_R\left[J_s^2\right] + \boldsymbol{M}_R\int_{t_0}^{t_{\mathrm{cycle}}}\left(\boldsymbol{M}_{\sigma}\frac{\partial \boldsymbol{a}(t)}{\partial t}\right)^2 \mathrm{d}t \tag{8}$$

The iron loss in the cores could be obtained by the Bertotti's equations [16]

$$\begin{aligned} \boldsymbol{q}_I(m) &= \boldsymbol{q}_h(m) + \boldsymbol{q}_c(m) + \boldsymbol{q}_e(m) \\ &= V(m)\left[k_h f B_p^x\right] + V(m)\left[k_c f^2 B_p^2\right] + V(m)\left[k_e f^{1.5} B_p^{1.5}\right] \end{aligned} \tag{9}$$

where $\boldsymbol{q}_h$, $\boldsymbol{q}_c$, and $\boldsymbol{q}_e$ are the hysteresis loss, the eddy-current loss of the iron cores, and k_h, k_c, and k_e are the constants, f the frequency.

C. 3-D Fluidic Model

The equations modeling the fluid flow consist of the continuity equation and the momentum conservation equations. The former one emphasizes the continuity of the fluid as

$$\boldsymbol{K}_x\boldsymbol{u} + \boldsymbol{K}_y\boldsymbol{v} + \boldsymbol{K}_z\boldsymbol{w} = 0 \tag{10}$$

where $\boldsymbol{K}_x$, $\boldsymbol{K}_y$, and $\boldsymbol{K}_z$ are the coefficient matrices stating the scale factors and the interface areas, and u, v, and w the velocities of the x, y, and z direction, respectively. The momentum conservation equations are in the following forms:

$$\boldsymbol{H}^{\mathrm{T}}\boldsymbol{M}_{\phi}\boldsymbol{G}\boldsymbol{u} + \boldsymbol{G}^{\mathrm{T}}\boldsymbol{M}_{\gamma}\boldsymbol{G}\boldsymbol{u} = \boldsymbol{K}_x\boldsymbol{p} \tag{11}$$

$$\boldsymbol{H}^{\mathrm{T}}\boldsymbol{M}_{\phi}\boldsymbol{G}\boldsymbol{v} + \boldsymbol{G}^{\mathrm{T}}\boldsymbol{M}_{\gamma}\boldsymbol{G}\boldsymbol{v} = \boldsymbol{K}_y\boldsymbol{p} \tag{12}$$

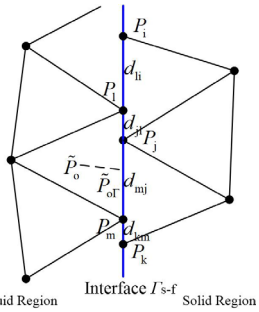

Fig. 3. Model of the fluid-solid interface.

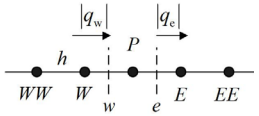

Fig. 4. 1-D structure grid.

$$\boldsymbol{H}^{\mathrm{T}}\boldsymbol{M}_{\phi}\boldsymbol{G}\boldsymbol{w}+\boldsymbol{G}^{\mathrm{T}}\boldsymbol{M}_{\gamma}\boldsymbol{G}\boldsymbol{w}=\boldsymbol{K}_{z}\boldsymbol{p} \tag{13}$$

where $\boldsymbol{H}$ is equal to $|\boldsymbol{G}|$.

D. Coupled Model

The models of the electromagnetic-thermal-fluidic problems are not the simple assembling of the individual fields. For the coupling of the 2-D electromagnetic field and the 3-D temperature field, due to the differences in the dimensions, the 2-D grids should be extended to the 3-D forms by the axial stretch of the model. Furthermore, the residual flux density and the coercive force are temperature-related properties [17]

$$B_r=\left[1+\left(T_{PM}-20\right)\kappa_{B_r}\right]\left(1-IL\right)B_{r20} \tag{14}$$

$$H_c=\left[1+\left(T_{PM}-20\right)\kappa_{H_c}\right]\left(1-IL\right)H_{c20} \tag{15}$$

Where T_{PM} is the temperature of the PMs, κ_{Br} and κ_{Hc} are the reversible temperature coefficients of the residual flux density and the coercive force, respectively, IL is the irreversible loss rate, B_{r20} and H_{c20} are the residual flux density and the coercive force at 20°C, respectively.

For the coupling of the fluid flow field and the thermal field, the heat transferred by convection should be mathematically modeled through the thermal equation of the fluid:

$$\boldsymbol{H}^{\mathrm{T}}\boldsymbol{M}_{\phi k}\boldsymbol{G}\boldsymbol{T}_f+\boldsymbol{G}^{\mathrm{T}}\boldsymbol{M}_{\lambda}\boldsymbol{G}\boldsymbol{T}_f=\boldsymbol{q}_V+\boldsymbol{q}_{bf} \tag{16}$$

where q_{bf} is the heat absorbed by the fluid from the fluid-solid interfaces. Since the solution domain of the fluid is complex, the meshes on the interfaces are not well-matched as shown in Fig. 3. The heat exchange through the interfaces covers:

$$q_i=\frac{(T_i+T_j)d_{jl}}{2\left[T_id_{jl}+T_j(d_{mj}+d_{jl})+T_kd_{mj}\right]}q_{bf} \tag{17}$$

$$q_j=\frac{(T_i+T_j)d_{jl}+(T_j+T_k)d_{mj}}{2\left[T_id_{jl}+T_j(d_{mj}+d_{jl})+T_kd_{mj}\right]}q_{bf} \tag{18}$$

$$q_k=\frac{(T_k+T_j)d_{mj}}{2\left[T_id_{jl}+T_j(d_{mj}+d_{jl})+T_kd_{mj}\right]}q_{bf} \tag{19}$$

E. Model Modification

Equation (11)-(13) and (16) are obtained through the central difference scheme. Take a 1-D structured grid as an example, as shown in Fig. 4, the x-directional accelerated velocity is

$$a_{Px}=\frac{-\frac{1}{2}|q_w|\left(u_P+u_W\right)+\frac{1}{2}|q_e|\left(u_P+u_E\right)}{V_P} \tag{20}$$

Where q_w and q_e are the flow rate passing through the w and e faces, respectively. Once the grids are uniformly distributed, the diagonal elements of the acceleration matrix are close to zero, thus making the equations hard to be solved. The variable ordered upwind schemes could be used to surmount the negative definition, but the matrices are still asymmetric. To conquer the problems, a first-ordered error is introduced

$$\begin{aligned}a_{Px}&=\frac{q\left(u_e-u_w\right)}{V_P}\\&=\frac{\frac{1}{2}q\left(u_E-u_W\right)-\frac{1}{2}q\left[\left(\left.\frac{\partial u}{\partial x}\right|_e-\left.\frac{\partial u}{\partial x}\right|_w\right)\right]h-q\left.\frac{\partial u}{\partial x}\right|_e h}{V_P}+O_{P1}(h)\\&=\frac{\frac{1}{2}q\left(u_E-u_W\right)-\frac{1}{2}q\left.\frac{\partial^2 u}{\partial x^2}\right|_P h^2-q\left.\frac{\partial u}{\partial x}\right|_e h}{V_P}+O_{P2}(h)\end{aligned} \tag{21}$$

The velocities of w and e faces are added with 1st order error.

$$\begin{cases}u_e=\frac{1}{2}\left(u_E+u_P\right)-\frac{3}{2}\left.\frac{\partial u}{\partial x}\right|_e h+O_e(h)\\u_w=\frac{1}{2}\left(u_W+u_P\right)-\frac{1}{2}\left.\frac{\partial u}{\partial x}\right|_w h+O_w(h)\end{cases} \tag{22}$$

The matrix formed (11)-(13) and (16) can be modified as

$$\boldsymbol{G}^{\mathrm{T}}\boldsymbol{M}_{\phi}\boldsymbol{G}\boldsymbol{u}+\boldsymbol{G}^{\mathrm{T}}\boldsymbol{M}_{\gamma}\boldsymbol{G}\boldsymbol{u}=\boldsymbol{K}_{x}\boldsymbol{p} \tag{23}$$

$$\boldsymbol{G}^{\mathrm{T}}\boldsymbol{M}_{\phi}\boldsymbol{G}\boldsymbol{v}+\boldsymbol{G}^{\mathrm{T}}\boldsymbol{M}_{\gamma}\boldsymbol{G}\boldsymbol{v}=\boldsymbol{K}_{y}\boldsymbol{p} \tag{24}$$

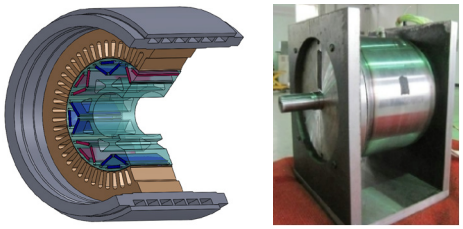
Fig. 5. Model of the fluid-solid interface.

TABLE I
MAIN DIMENSIONS AND DESIGN PARAMETERS

Parameters and Dimensions	Value
Rated power (kW)	20
Rated speed (rpm)	4500
Number of poles	4
Number of stator slots	48
Stator outer diameter (mm)	194.0
Rotor outer diameter (mm)	125.6
Air gap length (mm)	0.7
Axial length (mm)	75.0

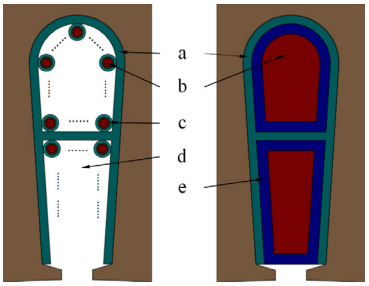

Fig. 6. Equivalent structure of a coil during calculation, which are (a) insulation sheet, (b) copper, (c) wire insulation, (d) air, (e) equivalent insulation.

$$\boldsymbol{G}^{\mathrm{T}}\boldsymbol{M}_{\phi}\boldsymbol{G}\boldsymbol{w}+\boldsymbol{G}^{\mathrm{T}}\boldsymbol{M}_{\gamma}\boldsymbol{G}\boldsymbol{w}=\boldsymbol{K}_{z}\boldsymbol{p} \tag{25}$$

$$\boldsymbol{G}^{\mathrm{T}}\boldsymbol{M}_{\phi k}\boldsymbol{G}\boldsymbol{T}_{f}+\boldsymbol{G}^{\mathrm{T}}\boldsymbol{M}_{\lambda}\boldsymbol{G}\boldsymbol{T}_{f}=\boldsymbol{q}_{V}+\boldsymbol{q}_{bf} \tag{26}$$

Equation (23)-(26) are positive defined and symmetric. Due to the implantation of a $(\partial u/\partial x)h$ shaped error into the mathematical model as shown in (21) and (22), the modified model is capable to the problems with small speed differences.

III. Coupled Analysis and Validation

To predict the temperature distribution of PMSMs, an interior PMSM is taken as a prototype during numerical and experimental analyses. The basic structure of the machine is shown in Fig. 5, and the basic parameters are shown in Table I.

A. Fundamental Assumptions

To obtain fine accuracy, the assumptions are as follows:

1) Considering the symmetry, a 1/8 model is employed.

2) In Fig. 6, conductors are modeled as uniform copper bars. The insulation, vanish and air in small cracks are gathered together and filled up the slots evenly [18].

3) The end windings are regarded as straight conductors with insulation wrapped outside to simplify the meshing process. In the real model, the end windings are overlapped by the flanks, and the major heat generated in the end windings is dissipated through the top and bottom faces. During calculation, the side faces of the end windings are regarded as adiabatic surfaces while the top and bottom faces are convective. By this simplification, the heat of the end windings transferred through the air enclosed in the end-caps to the profiles of the stator core is decreased due to the increased distances. However, the modeling error caused by the assumption is small since the air temperature is rather low with the well established water-cooling system.

4) The heat transferred by radiation is ignored.

B. Numerical Results

Equation (5)-(6), (10), and (23)-(26) based models are employed to analyze the coupled electromagnetic-thermal-fluidic fields of the PMSM. The electromagnetic field as the weakly coupled part is firstly computed, and the electromagnetic losses calculated and tested are compared in Fig. 7.

The losses are used as the heat sources during the directly coupled thermal-fluidic analyses. Since the fluid flow distribution is hard to be tested, the temperature rise of the machine is taken as the criterion. The temperature rise distribution of the whole machine is shown in Fig. 8 (a). Fig. 8(b) and (c) demonstrate the temperature rise distributions of the windings and the PMs calculated, respectively. And the temperature rise of the rotor part is higher than that of the stator part, because the stator core is directly connected to the water-cooled machine enclosure while the heat generated in the rotor core and the PMs is hard to be dissipated. In Fig. 8(b), the maximum temperature rise of the windings occurred in the end-regions since the conductive cooling performance of the stator core is better than the heat transferred through convection by the air enclosed in the end-caps.

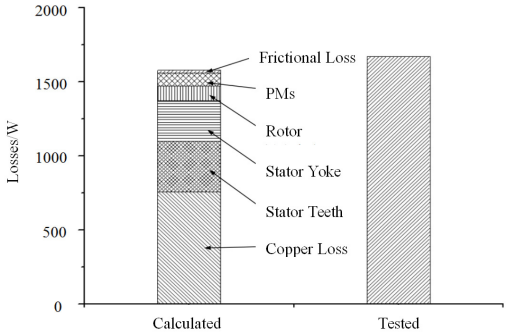

Fig. 7. Losses calculated and tested.

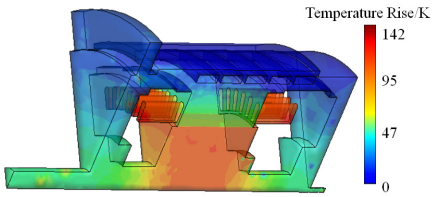

(a) the whole machine

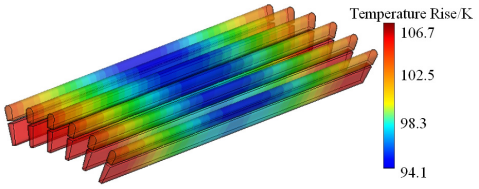

(b) the windings

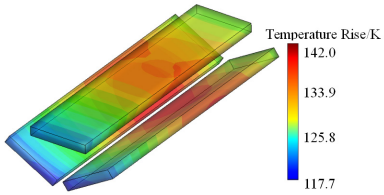

(c) the PMs

Fig. 8. Temperature rise distribution.

C. Experimental Validation

TABLE II
TEMPERATURE RISE CALCULATED AND TESTED

Position	End-Winding	PM
Temperature rise tested	111.4K	149.5K
Temperature rise calculated	101.8K	137.9K
Error	8.64%	7.75%

TABLE III
OUTPUT TORQUE DESIGNED AND TESTED UNDER RATED SPEED

Condition	Torque
Designed	42.48N·m
Thermal-state tested	40.70N·m
Difference	4.19%

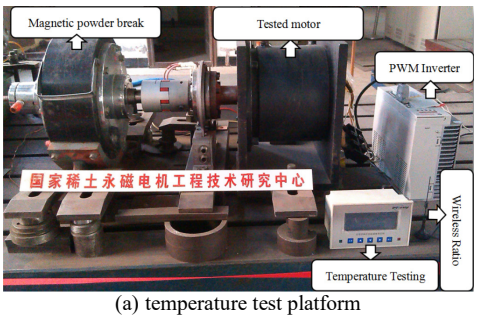

(a) temperature test platform

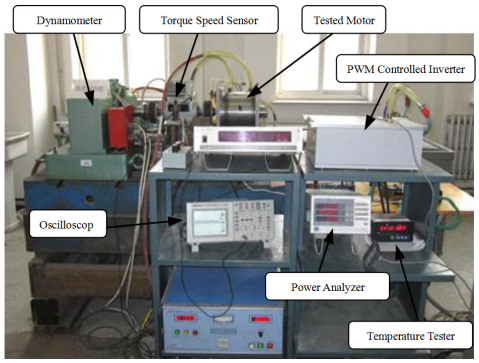

(b) performance test platform

Fig. 9. Experimental setup.

Experiments were carried out to measure the motor temperature distribution at the rated output power by the experimental platform shown in Fig. 9. Wireless thermal sensitive resistors were buried underneath the end-windings and beneath the PMs, and the temperatures were measured to verify the numerical simulations. Table II tabulates the temperature rises of the computed results and the experimental ones. The calculation errors caused by the model modification and the assumption are less than 9%.

IV. Conclusion

The multi-physical analysis techniques based on the CM are presented including the coupled relations between electromagnetic, thermal, and fluidic fields. In order to improve the positive definiteness and the symmetry of the global stiffness matrix to reduce the computational burden, the equations coupling the fluid flow and the temperature are modified in this paper with a 1st order error added to the acceleration equations. The numerical results can show good accuracy compared with the experimental ones.

References

[1] N. Z. Popov, S. N. Vukosavic, and E. Levi, "Motor temperature monitoring based on impedance estimation at PWM frequencies," *IEEE Trans. Energy Convers.*, vol. 29, no. 1, pp. 215-223, Mar. 2014.

[2] R. C. Gleichman, "Failure modes and field testing of medium-voltage motor windings," *IEEE Trans. Ind. Appl.*, vol. 38, no. 5, pp. 1473-1476, Sept./Oct. 2002.

[3] S. D. Wilson, P. Stewart, and B. P. Taylor, "Methods of resistance estimation in permanent magnet synchronous motors for real-time thermal management," *IEEE Trans. Energy Convers.*, vol. 25, no. 3, pp. 698-707, Sept. 2010.

[4] A. J. Grobler, S. R. Holm, and G. V. School, "A two-dimensional analytic thermal model for a high-speed PMSM magnet," *IEEE Trans. Ind. Electron.*, vol. 62, no. 11, pp. 6756-6764, Nov. 2015.

[5] X. Z. Huang, L. Y. Li, B. Zhou, C. M. Zhang, and Z. R. Zhang, "Temperature calculation for tubular linear motor by the combination of thermal circuit and temperature field method considering the linear motion of air gap," *IEEE Trans. Ind. Electron.*, vol. 61, no. 8, pp. 3923-3931, Aug. 2014.

[6] E. Tonti, "Finite formulation of electromagnetic field," *IEEE Trans. Magn.*, vol. 38, no. 2, pp. 333-336, Mar. 2002.

[7] E. Tonti, "The reason for analogies between physical theories," *Appl. Math. Model.*, vol. 1, no. 1, pp. 37-50, June 1976.

[8] E. Tonti, "Why starting from differential equations for computational physics," *J. Comput. phys.*, vol. 257, no. 1, pp. 1260-1289, Jan. 2014.

[9] P. Alotto, F. Freschi, and M. Repetto, "Multiphysics problems via the cell method: the role of Tonti diagram," *IEEE Trans. Magn.*, vol. 46, no. 8, pp. 2959-2962, Aug. 2010.

[10] M. Marrone, R. Mittra, "A theoretical study of the stability criteria for hybridized FDTD algorithms for multiscale analysis," *IEEE Trans. Antennas Propag.*, vol. 52, no. 8, pp. 2158-2167, Aug. 2004.

[11] P. Alotto, M. Bullo, M. Guarnieri, and F. Moro, "A coupled thermo-electromagnetic formulation based on the cell method," *IEEE Trans. Magn.*, vol. 44, no. 6, pp. 702-705, June 2008.

[12] M. Bullo, V. D. Ambrosio, F. Dughiero, and M. Guarnieri, "A 3-D cell method formulation for coupled electric and thermal problems," *IEEE Trans. Magn.*, vol. 43, no. 4, pp. 1197-1200, Apr. 2007.

[13] P. Alotto, G. Gruosso, F. Moro, and M. Repetto, "A boundary integral formulation for eddy current problems based on the cell method," *IEEE Trans. Magn.*, vol. 44, no. 6, pp. 770-773, June 2008.

[14] O. Biro, and K. Preis, "On the use of the magnetic vector potential in the finite element analysis of three-dimensional eddy currents," *IEEE Trans. Magn.*, vol. 25, no. 4, pp. 3145-3159, July 1989.

[15] P. Alotto, M. Repetto, F. Freschi, and C. Rosso, *The Cell Method for Electrical Engineering and Multiphysics Problems: An Introduction*, 1st ed., Berlin: Springer-Verlag, 2013, pp. 83-85.

[16] G. Bertotti, "General properties of power losses in soft ferromagnetic materials," *IEEE Trans. Magn.*, vol. 24, no. 1, pp. 621-630, Jan. 1988.

[17] R. Y. Tang, *Modern Permanent Magnet Machines: Theory and Design*, 1st ed., Beijing: China Machine Press, 2011, pp. 215-227.

[18] Q. F. Lu, X. M. Zhang, Y. Chen, X. Y. Huang, Y. Y. Ye, and Z. Q. Zhu, "Modeling and investigation of thermal characteristics of a water-cooled permanent-magnet linear motor," *IEEE Trans. Ind. Appl.*, vol. 51, no. 3, pp. 2086-2096, May/Jun. 2015.

Gaojia Zhu received the Ph.D. degree in electrical engineering from National Engineering Research Center for Rare-earth Permanent Magnet Machines, Shenyang University of Technology, Shenyang, China, in 2017. He is currently a lecturer in School of Electrical Engineering and Automation, Tianjin Polytechnic University, Tianjin, China, his research direction is the multi-physics coupled analyses and optimal design of electrical machines.

Xiaoming Liu received the Ph.D. degree in electrical engineering from Shenyang University of Technology, Shenyang, China, in 2003. She is currently a Professor of electrical engineering and the Head of the School of Electrical Engineering and Automation, Tianjin Polytechnic University, Tianjin, China. Research direction covers the design and optimization of electrical apparatus, high voltage and insulation technology.

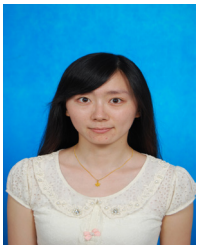

Longnv Li received the Ph.D. degree in electrical engineering from National Engineering Research Center for Rare-earth Permanent Magnet Machines, Shenyang University of Technology, Shenyang, China, in 2016. She is currently a lecturer and post-doctor at School of Electrical Engineering and Automation, Tianjin Polytechnic University, Tianjin, China.

The research interests are the multi-physics coupled analyses and optimal design of electromagnetic devices.

Hai Chen received the B.E. degree from Beijing University of Aeronautics and Astronautics, Beijing, China, in 1990, and the M.E. degree from Shenyang University of Technology, Shenyang, China, in 1993, all in mechanics. He is currently an Engineer of Tianjin Polytechnic University, Tianjin, China. Research interest is the design of electromagnetic devices.

Jianguo Zhu (S'93–M'96–SM'03) received the B.E. degree from Jiangsu Institute of Technology, Zhenjiang, China, in 1982, the M.E. degree from Shanghai University of Technology, Shanghai, China, in 1987, and the Ph.D. degree from the University of Technology Sydney (UTS), Sydney, Australia, in 1995, all in electrical engineering. He is currently a Professor of electrical engineering and the Head of the School of Electrical and Information Engineering at The University of Sydney, Australia. His current research interests include electromagnetics, magnetic properties of materials, electrical machines and drives, power electronics, and green energy systems.